https://doi.org/10.17221/26/2026-SWR

Reduction in hydraulic conductivity for high burn severity soils begins after the first rainfall event: Results from laboratory-scale rainfall simulation experiments

Nana Afua Gyau Frimpong[1], *Jacob Huerta*[2], *Ryan Webb*[1]*

[1]*Department of Civil & Architectural Engineering and Construction Management, University of Wyoming, Laramie, Wyoming, USA*

[2]*Department of Mechanical Engineering, University of Wyoming, Laramie, Wyoming, USA*

**Corresponding author: Ryan.Webb@uwyo.edu*

Citation: Frimpong N.A.G., Huerta J., Webb R. (2026): Reduction in hydraulic conductivity for high burn severity soils begins after the first rainfall event: Results from laboratory-scale rainfall simulation experiments. Soil & Water Res., 21: 169–178.

Abstract: Wildfires can greatly impact the hydraulic properties of soil. This study aims to utilise laboratory experiments to simulate burned soil conditions under a range of slope angles and rainfall intensities to address the research question: How does the presence of ash after the first rainfall event impact the hydraulic properties of burned soil in complex terrain? Sandy loam soils for this study were sourced from a mixed conifer forested area in the San Juan Mountains of southern Colorado, USA. Measurements of soil hydraulic properties in experimental microplots were taken (1) before burning, (2) after burning, and (3) 24 hours after a rainfall simulation. A total of 15 experimental microplots with ash applied were run through rainfall simulations at slope angles ranging from 10° to 30°. Results found ash eroded had no significant relation to slope angle, but there was a significant reduction in field saturated hydraulic conductivity of samples with ash after rainfall simulations. To build on the findings presented here, future research should conduct field-based studies across various ecosystems and soil types to observe post-fire soil changes over time.

Keywords: post-wildfire hydrology; soil hydraulic conductivity; soil sealing; surface crust

Wildfires pose an increasing risk for mountainous environments worldwide. In particular, the western United States has seen an increase in the frequency and magnitude of wildfires in recent years (McKenzie et al. 2004; Dennison et al. 2014; Westerling 2016). Not only do wildfires create an immediate threat of burning forests and infrastructure, but the areas affected experience increased runoff generation that can lead to dangerous flooding (Moody et al. 2008, 2013; DeLong et al. 2018; Saxe et al. 2018; Wilson et al. 2018) and water quality issues (Smith et al. 2011; Hallema et al. 2018). These can be costly for municipalities and landowners to mitigate and recover from, with large uncertainties in estimates during planning efforts (Benavides-Solorio & MacDonald 2001; Fernandez & Vega 2018; Schmeer et al. 2018). These uncertainties need to be better constrained for future efforts in wildfire damage mitigation and recovery (Webb et al. 2023). This is especially true in the face of global climate change that predicts that wildfires will worsen over the coming years (Abatzoglou & Williams 2016).

A major component of uncertainty in wildfire effects is the altered soil properties that occur in a highly

Supported by the United States National Science Foundation, Grant No. 2136339.

https://doi.org/10.17221/26/2026-SWR

heterogenous manner across a landscape (Pelletier & Orem 2014; Moody et al. 2016; Ebel & Martin 2017; McGuire et al. 2018). Changes to soil properties after a wildfire control the magnitude of hydrologic response to precipitation events. Work has been conducted to understand the change in physical properties of soil (Burgy & Scott 1952; Leon et al. 2013; Ebel & Moody 2017; Wieting et al. 2017; Perkins et al. 2022) and the chemical make-up of ash materials (Cerrato et al. 2016; Rahman et al. 2018). However, less is understood concerning the mobility of ash materials into soil and the effects on soil sealing processes and resulting hydrologic fluxes immediately after a fire, particularly at different slope angles. Most of the work in this discipline has been conducted in laboratory settings for one-dimensional (vertical) investigations without a sloping surface (Wieting et al. 2017; Kim et al. 2022) or field settings where observations are limited to when investigators can enter the site, often after these effects have dissipated (Onda et al. 2008; Schmeer et al. 2018). There remains a gap in understanding the way hydrologic fluxes occur at and across the soil-ash interface on hillslopes in complex terrain immediately following a fire.

Infiltration on hillslopes is a key component of the hydrologic cycle that determines runoff generation for streamflow. Infiltration rate reduction following wildfire is the primary cause for increased runoff and erosion. However, the specific physical processes that alter soil characteristics are less understood (Larsen et al. 2009; Leon et al. 2013; Ebel & Moody 2017; Thomaz 2018). There are generally four physical properties of soil that affect infiltration after a wildfire: soil-water repellence, changes in soil structure, loss of organic matter, and soil sealing (including pore clogging and ash crust formation). Soil sealing is one of the less studied processes of post-wildfire hydrologic impacts, likely because of the rapid occurrence and rapid deterioration of the seal following a fire (Onda et al. 2008; Woods & Balfour 2008; Ebel & Moody 2017). However, this short timeline of soil sealing immediately after a wildfire is also the time of highest risk for high damage flooding due to the lack of vegetation. The publications that do address soil sealing show that the depth of ash, type of ash, rainfall intensity, and removal of the ash layer are important variables that affect soil sealing processes (Cerda & Doerr 2008; Onda et al. 2008; Woods & Balfour 2008; Larsen et al. 2009; Bodi et al. 2012).

Until recently, studies determined the hillslope-scale hydraulic properties of post-wildfire soils and ash separately, conceptualising the hillslope as a two-layer system of soil and ash (Leon et al. 2013; Ebel & Martin 2017). This is an effective approach to determine the storage capacity and runoff characteristics of the system during the first precipitation event after a fire. However, the two-layer system rapidly evolves as the hydraulic properties of the ash layer change in reaction with water (Onda et al. 2008) and movement of ash materials across the soil-ash interface occurs, creating a new surface boundary layer (Woods & Balfour 2008; Larsen et al. 2009; Balfour et al. 2014; Kim et al. 2022). This process has been documented and conceptualised based on observations at individual sites and the net effects on runoff when post-wildfire soils and ash are studied together (Moody et al. 2013; Vieira et al. 2015; Ebel & Moody 2017; Saxe et al. 2018).

Therefore, this study aims to utilise laboratory experiments to further understand the effects of soil sealing processes on post-fire hydrology across various slope angles. Laboratory experiments were designed to simulate burned soil conditions under a range of slope angles and rainfall intensities to address the research question: How does the presence of ash after the first rainfall event impact the hydraulic properties of burned soil in complex terrain? Specifically, this study aims to improve our understanding of soil hydraulic properties immediately following the first post-wildfire rainstorm.

MATERIAL AND METHODS

Soils source. The soils for this study were sourced from a mixed conifer forested area within a private ranch in the headwaters of the Navajo River Basin, in the San Juan Mountains of southern Colorado USA. The soil type used for this study is a sandy loam according to the USDA soil taxonomy classification system (5% clay, 27% silt, and 68% sand). The soil type for the area is predominantly Castelleia loam, which is a well-drained soil derived from igneous rock and/or complex landslide deposits derived from latite over sandstone and shale. The Köppen–Geiger Climate Classification of the area is considered a snow climate, fully humid, and with cool summers (Kottek et al. 2006). The tree species in the area include ponderosa pines, aspen, white fir, Douglas fir, blue spruce, lodgepole pine, and Engelmann spruce. In situ soil samples with dimensions of 50 × 30 × 20 cm were collected from the upper 20 cm of soil at the site. Samples were dug out with

https://doi.org/10.17221/26/2026-SWR

a hand trowel in slightly larger dimensions to allow for sculpting to an exact fit when placed in the experimental apparatus. Vegetation roots and leaves were kept intact for the purpose of this study. Soil samples were arranged in microplots of the same dimensions for the experiments of the study. Microplots contained 20 cm of gravel below the samples to allow free drainage and included a spout at the soil surface height to monitor surface runoff from rainfall experiments.

Soil preparation. To investigate post-fire soil dynamics, experiments were carried out in a controlled laboratory environment on prepared soil samples within the microplots previously described. To simulate wildfire conditions, propane torches were used to expose soil surfaces and vegetation to a simulated high severity fire. Torches were applied for approximately 20–30 min to each microplot elevating soil surface temperatures to between 450 °C and 500 °C, monitored using a Liseran infrared handheld thermometer. Temperatures within the soil profile were not monitored. Following the burning simulation, approximately 1 cm of ash (455 g) was evenly distributed across the microplot using a one mm sieve, ensuring a consistent particle size and uniform spread. This ash, derived from lodgepole pine burned in a controlled environment, was applied to mimic post-wildfire conditions under a high-intensity canopy burn. Following the application of ash, microplots were placed in custom designed frames to allow slope angles ranging from 0°–30° within the rainfall simulator.

Additionally, we prepared two control groups of soil samples. Control group A was soil samples that remained undisturbed and went through the same testing procedures as all soil samples. Control group B was soil samples that were burned in the same method described above, but no ash was applied to the surface. In this manner, the control groups allow us to identify if any changes in soil properties are a result of the experimental procedure, the burning of the soil, or the presence of ash on the surface.

Rainfall simulator. Rainfall simulators allow comparisons of soil conditions across different sites (Humphry et al. 2002). The rainfall simulator used in our experimental set-up followed a similar design described by Humphrey et al. (2002) and Schoener and Stone (2019) with an area of approximately 2 m^2 (Figure 1). To achieve an appropriate fall velocity of raindrops, a single nozzle was positioned three meters above the soil samples. We used the Spraying Systems Co. model HH-17WSQ (Spraying Systems Co., USA), chosen for its ability to produce droplets closely resembling the size of natural raindrops (1–5 mm), and the desired

Figure 1. Images of the rainfall simulator (A) showing height of nozzle above microplots and the ability to independently tilt experimental microplots, and (B) an active rainfall simulation for the Control A group (undisturbed samples).

https://doi.org/10.17221/26/2026-SWR

rainfall intensities (Schoener & Stone 2019), allowing the simulation of realistic rainfall conditions. Rainfall simulations were conducted for 30-min experiments with rainfall intensities from approximately 15 to 65 mm/h, representing a range from 1-year to 50-year storms, respectively. To measure the amount of material eroded from the surface, three lidded buckets were placed at the open ends of the rainfall microplots. These buckets collected the eroded ash and soil, which were weighed to calculate the amount of material eroded. Meanwhile, three ECRN 100 high-resolution rain gauges (Meter Group, Inc., USA) were positioned at the opposite ends of the microplots to measure rainfall intensity. The rainfall simulator was shown to provide relatively homogeneous rainfall over the three experimental plots in the data from these rain gauges. We adjusted the rainfall intensity by regulating pressure on the inflow pipe. A total of 24 30-minute experiments were conducted, with varying conditions such as slope angles and rainfall intensities (Table S1 in Electronic Supplementary Material).

Hydraulic properties of soil. Measurements of soil hydraulic properties for each microplot were taken (1) before burning, (2) after burning, and (3) 24 h after the rainfall simulation. A mini disk infiltrometer (MDI) was employed to measure unsaturated hydraulic conductivity that we refer to as field saturated hydraulic conductivity (K_{fs}) due to measurements being made at tensions less than 5 cm that may be considered near saturation. We also utilised the ethanol drop test to assess soil water repellence in an alternating pattern as depicted in Figure 2. This resulted in three measurements of K_{fs} and three measurements of repellence per microplot at each stage of the experiments.

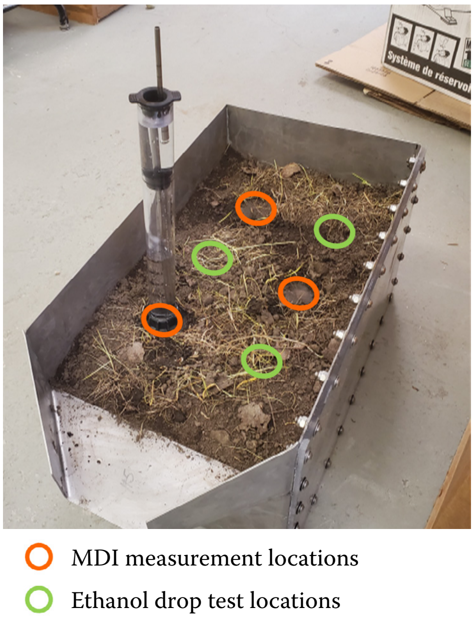

Figure 2. Image of approximate locations for the mini disk infiltrometer (MDI) measurement and ethanol drop test measurement locations with an active MDI measurement taking place

We applied the MDI procedures as outlined in the product manual (Meter Group, Inc.). We applied suction ranging from 1.5 to 4 cm based on the rate of infiltration to allow accurate recording of reservoir levels. This range of suctions has minimal impact on the final K_{fs} estimate. The amount of water infiltrating the soil from the reservoir was recorded at regular intervals, and K_{fs} values were calculated following the method described by (Zhang 1997). Per these methods, cumulative infiltration (I) can be represented as a function combining two key parameters:

$$I = C_1\sqrt{t} + C_2 t \qquad (1)$$

where:
C_1 – soil sorptivity (m/s);
C_2 – hydraulic conductivity (m/s$^{0.5}$);
t – time (s).

From this K_{fs} is derived through the relationship

$$K_{fs} = \frac{C_2}{A} \qquad (2)$$

where:
C_2 – the slope of the cumulative infiltration vs the square root of time;
A – a parameter incorporating van Genuchten characteristics with infiltrometer parameters using the following equations:

$$A = \frac{11.65\left(n^{0.1}-1\right)\exp\left[2.92(n-1.9)\alpha h_0\right]}{\left(\alpha r_0\right)^{0.91}}, \text{ for } n \geq 1.9 \qquad (3)$$

$$A = \frac{11.65\left(n^{0.1}-1\right)\exp\left[7.5(n-1.9)\alpha h_0\right]}{\left(\alpha r_0\right)^{0.91}}, \text{ for } n < 1.9 \qquad (4)$$

where:
r_0 – the disk radius (2.25 cm);
h_0 – the applied suction;
n, α – the van Genuchten parameters for the soil texture as defined in Carsel and Parrish (Carsel & Parrish 1988).

https://doi.org/10.17221/26/2026-SWR

To assess soil water repellence, we used the molarity of an ethanol droplet test (Watson & Letey 1970; Doerr 1998). This test involved placing 5 drops of ethanol solutions with gradually increasing concentrations on the soil surface. The degree of water repellence was determined by identifying the minimum ethanol concentration that could penetrate the soil within 3–5 seconds. Classifications in this system range from 36% ethanol, considered to be "extremely hydrophobic", to 0% ethanol considered "very hydrophilic" (Doerr 1998).

Impact of ash depth. To test the effect of ash depth on K_{fs} after the first rainfall post-wildfire, we conducted further testing using re-packed soil in a 250 cm^3 stainless steel ring. Samples were re-packed to ensure uniformity between the soil, reducing macropore flow. Each sample measured an inner diameter of 8 cm and a height of 5 cm. Samples were prepared to achieve a dry bulk density of 0.807 g/cm^3 to match in situ samples. The amount of soil was adjusted with varying depth of ash so that all samples were 5 cm in height. All experiments were conducted in triplicate with ash depths ranging from 0 to 1 cm in 0.25 cm increments. The samples with no ash served as control samples. Similar procedures as the microplot experiments were conducted to collect MDI measurements (1) before burning, (2) after burning, and (3) after ash was applied and samples experienced a 30-min simulated rainfall at an intensity of ~40 mm/h, representing the average rainfall rate in the micro-plot experiments.

Statistical analysis. In our analysis, we employed both the rank-sum test (also known as the Mann-Whitney U or Wilcoxon rank-sum test) and the t-test to determine significant differences between independent groups pre-burn, post-burn, and post-rainfall. To determine the appropriate statistical test, we assessed the normality of the data using the Shapiro-Wilk test at a 0.05 significance level. If the data met the normality assumption, a t-test was used; otherwise, the Wilcoxon test was applied. The Wilcoxon rank-sum test, a non-parametric method developed by Mann and Whitney (1947) and further refined by Wilcoxon (1992), is beneficial for data that do not follow a normal distribution or when dealing with ordinal data. In contrast, the t-test is used to compare the means of two groups, assuming normally distributed data. By utilising both tests, we ensured that our analysis was robust across varying data distributions. Lastly, we conducted linear regression analyses to determine the influence, if any, of slope angle and rainfall intensity on material eroded as well as the influence of ash depth on the change in K_{fs} after rainfall.

RESULTS

Ash retention. A total of 15 experimental microplots with ash applied were run through rainfall simulation experiments at slope angles ranging from 10 ° to 30 °. We assessed the degree of material erosion for these 30-min rainfall events through linear regression, finding no significant relation for the amount of eroded material to slope angle (P-value = 0.92) or rainfall intensity (P-value = 0.26). This lack of statistical significance indicates random erosion rates that ranged from 0.2 to 25.2 g (Table 1). Furthermore, all microplots remained completely ash-covered with no bare soil after rainfall simulations and eroded material collected was almost entirely ash. These values represent low percentages of the total ash applied (455 g) ranging from 0.04% to 5.5% showing that all tests retained the majority of ash even at high precipitation rates and slopes of 30°.

Hydraulic properties of soil. Repellence tests resulted in approximately 12% of the tests showing some level of hydrophobicity prior to burning (4% very strongly hydrophobic, 8% moderately hydrophobic, 17% hydrophilic, and 71% very hydrophilic). After

Table 1. Results of ash erosion of all microplot experiments that had ash applied prior to 30-minute rainfall simulations

Slope angle (°)	Rainfall rate (mm/h)	Ash eroded	
		(g)	(%)
10	24.4	0.6	0.1
10	46	0.5	0.1
10	64.4	23.5	5.2
20	23.2	0.4	0.1
20	37.6	0.5	0.1
20	45.6	8.1	1.8
30	17.6	23.6	5.2
30	28.8	3.5	0.8
30	46	25.2	5.6
30	24.4	0.4	0.1
30	24	0.5	0.1
30	40.4	0.6	0.1
30	26.8	0.2	0.04
30	40	0.2	0.05
30	56	4.0	0.9

https://doi.org/10.17221/26/2026-SWR

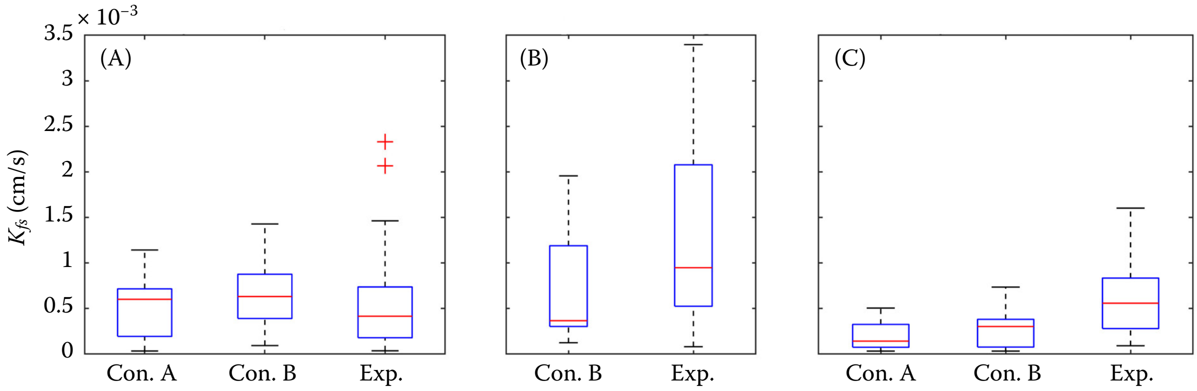

Figure 3. Results of the mini disk infiltrometer (MDI) measurements for soil samples in microplots for field saturated hydraulic conductivity (K_{fs}): (A) pre-disturbance, (B) after soils were burned and ash applied (for experimental soils only), and (C) after rainfall simulations; shown are results for the control A group (Con. A, undisturbed soil), control B group (Con. B, burned with no ash), and the experimental group (Exp., burned and ash applied)

burning, only 4% of all soils showed any level of hydrophobicity (4% slightly hydrophobic, 96% very hydrophilic). After the rainfall simulations, all soils tested were hydrophilic (8% hydrophilic, 92% very hydrophilic). This low level of hydrophobicity is due to the high intensity of burning simulated in these experiments.

In total, we tested soil samples in 24 microplots (3 Control A, 6 Control B, and 15 Experimental). Each microplot received three MDI observations for each stage of the procedures, resulting in 72 measurements pre-disturbance, 63 after burning, and 72 after rainfall. The MDI results showed no statistical difference between the control and experimental groups in pre-disturbance measurements. However, after the rainfall simulations, the experimental group showed a statistically significant difference compared to both the control A group (P-value = 0.001) and the control B group (P-value = 0.0003). Both control groups did not show a significant difference to one another after rainfall simulations indicating the difference in the experimental group is a result of the ash. The experimental group experienced a mean change in K_{fs} of $+3.6 \times 10^{-5}$ cm/s (Figure 3). After burning, the control B and experimental groups both saw an increase in variability of K_{fs} (Figure 3B).

Impact of ash depth. A total of 11 soil samples provided results from MDI measurements with ash depth ranging from 0 to 1 cm. The results of this test showed no effect of ash depth on the final K_{fs} after rainfall (Figure 4). Linear regression analysis resulted in an adjusted r-squared value of 0.06 and a P-value of 0.23 indicating no relation between ash depth and K_{fs}.

DISCUSSION

This study implementing soil samples in laboratory-scale experiments found that the slope angle and rainfall intensity did not influence the amount of ash that eroded in microplots with approximately 0.15 m^2 area. We did find, however, that the presence of ash results in significant differences in K_{fs} after the rainfall simulations when compared to control groups

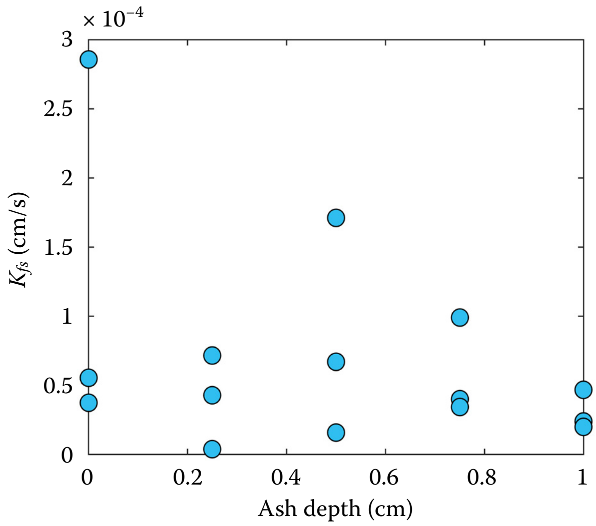

Figure 4. Results of mini disk infiltrometer (MDI) field saturated hydraulic conductivity (K_{fs}) measurements for re-packed soil samples after rainfall simulations with varying depths of ash

https://doi.org/10.17221/26/2026-SWR

that did not have ash applied to the soil surface. The depth of ash (up to 1 cm), however, was not found to influence to K_{fs} values after rainfall.

The small plot size of the microplots (0.15 m²) restricted the development of concentrated surface runoff, which may explain the lack of influence from slope angle and rainfall intensity in ash erosion. We did not observe any concentrated surface flow in the form of rills on our microplots during rainfall simulations. Small plots limit the upslope contributing area and fail to create concentrated flow channels necessary for erosion to occur. Previous studies have found that erosion dynamics are unaffected by slope in plots under 1 m^2 (Chaplot & Bissonnais 2000). Thus, our results predominantly reflect the influence of inter-rill erosion from the impact of rain drops on the ash surface. Future research could utilise larger plots at the hillslope scale or artificially create rill flow in a laboratory setting to further explore erosion rates and the impact on K_{fs} after erosion occurs on slope angles previously shown to influence post-fire surface runoff (Doerr et al. 2006; Shakesby & Doerr 2006).

The statistically significant results found in the K_{fs} changes through our experiments can be explained by known effects from fire and rainfall on soils. In the pre-disturbed stage, K_{fs} values ranged from 3.4×10^{-5} to 2.3×10^{-3} cm/s, aligning with typical hydraulic conductivity values for sandy loam soils (Al-Dosary et al. 2019, 2022). However, we observed post-burn K_{fs} values increased significantly compared to pre-disturbed values (Figure 3B). While K_{fs} values tend to decrease after a fire, studies have also observed an increase in K_{fs} for both simulated wildfires (e.g., Wieting et al. 2017) and natural wildfire (e.g., McGuire et al. 2024; Martinez et al. 2025). We attribute this immediate increase to the combustion process, which likely increased soil porosity by removing organic matter and creating additional pore pathways, thereby enhancing water movement (Leslie et al. 2014). We qualitatively observed the removal of organic material and increased porosity in the burned soil. Additionally, the high temperatures imposed by our experiments of over 400 °C vaporise hydrophobic compounds from organic material, which tend to reduce K_{fs} after burning for lower severity burns (Moody et al. 2008). However, the depth of burning was confined to approximately 1 cm in the 20 cm soil profiles, indicating that these changes in K_{fs} are restricted to near the soil surface. After rainfall simulations, K_{fs} decreased significantly across samples. This reduction is likely due to raindrop impact, which can displace fine particles (such as ash) into pore spaces, clogging them and reducing effective flow pathways. This pore-clogging effect may be further exacerbated by surface sealing and crust formation due to the presence of ash that provides numerous additional fine particles for the pore-clogging process, as found by other studies (Kim et al. 2022).

Supporting our findings, other studies have also found that intense fires can temporarily increase infiltration rates by modifying pore structure in addition to the potential for surface sealing to develop over time, reducing infiltration (Doerr et al. 2000; Ebel et al. 2012). Multiple studies have observed that the soil-ash interface can promote water movement through increased water storage capacity in the ash layer, preferential flow-paths, and enhanced surface roughness promoting infiltration (Woods & Balfour 2010; Ebel et al. 2012; Bodí et al. 2014). However, these effects are often short-lived as ash particles eventually clog soil pores (Balfour & Woods 2013) and burned soil tends to undergo structural collapse and reduced porosity (Certini 2005), leading to reduced infiltration rates. Our results align with these other studies, suggesting that both ash and fine soil particles translocate into the soil matrix, leading to pore clogging and lower permeability (Debano 2000; Moody et al. 2016). As our results show, the surface sealing process begins rapidly after rainfall. Other studies show ash and fine soil particles consolidate on the surface, forming a low-permeability layer (Larsen et al. 2009; Stoof et al. 2010; Woods & Balfour 2010). Our findings indicate that this reduction in K_{fs} occurs wherever ash deposits are found on the soil from 0–1 cm in depth (Figure 4).

Limitations. It is also important to recognise the limitations of our study. These results do not translate directly to natural conditions due to some of the simplifications necessary to make laboratory-scale studies feasible. The lack of variability in soil texture, antecedent moisture conditions, and ash applications are just some examples of variables that we maintained consistent for our study. However, these conditions will vary both spatially and temporally in natural environments. Additionally, our use of a propane torch is a simplification of the natural conditions that a wildfire produces. Lastly, our study has limitations in the temporal changes that the soil and ash will undergo following a wildfire. Our analysis is limited to only 24 hours after

https://doi.org/10.17221/26/2026-SWR

the first rainfall event with no demonstration of the persistence or potential reversal of observed effects. While these simplifications were necessary to draw robust conclusions from our experiments and avoid too many variables to be feasibly tested, it does limit the direct applications on a natural hillslope. However, we believe that the microplots add complexity in surface roughness and slope angle that are not generally tested in the smaller samples often used in laboratory studies. Thus, our study begins to bridge the gap between the smaller-scale laboratory studies and hillslope scale processes, with limitations that may be further addressed in future studies.

Next steps. While our study highlights immediate changes in K_{fs}, longer-term patterns are likely to differ (e.g., Gerdes et al. 2024). Gerdes et al. (2024) investigated the long-term effects of high intensity burns one, three, and six years after burning, finding K_{fs} returns to similar values as unburned soils within the first year. Over longer periods, K_{fs} declined to lower than unburned surrounding soils due to further pore compaction and the gradual breakdown of organic matter. These findings suggest a complex temporal pattern in soil responses to fire: (1) an initial increase in K_{fs} due to newly formed pore pathways, (2) pore-clogging and soil sealing, and (3) further declines after three years as soil structure continues to change. Future research could focus on the interactions between fire intensity, soil compaction, and organic matter recovery across multiple time scales to better understand the full trajectory of post-fire hydraulic changes. Such insights could prove beneficial for predicting and managing post-fire watershed responses and mitigating soil erosion and runoff risks in fire-affected landscapes.

To build on the findings presented here, future research should conduct long-term, field-based studies across various ecosystems and soil types to validate results and observe post-fire soil changes over time. Additionally, it will be necessary to determine how the processes studied in this paper would differ for varying soil texture, antecedent moisture conditions, ash applications, range of slope angles, and burn severities to improve generalizability. Enhanced methodologies for measuring hydraulic conductivity in situ and studying the dynamics of hydrophobic layers over multiple wetting-drying cycles could also further refine understanding. Finally, future studies should explore the role of vegetation recovery and test erosion control strategies to better inform post-fire land management.

CONCLUSION

This study found that the slope angle and rainfall intensity did not influence the amount of ash that eroded in microplots with approximately 0.15 m^2 area. The depth of ash was also found to not influence K_{fs} for ash depths up to 1 cm. However, we did find that burning the soil and the presence of ash results in significant differences in K_{fs} after the rainfall simulations for our sandy loam soil. Pre-disturbance, we observed K_{fs} values ranging from 3.4×10^{-5} to 2.3×10^{-3} cm/s, with values increasing significantly after the soil was burned followed by a significant decrease after ash was applied and the microplots underwent 30-min rainfall simulations.

REFERENCES

Abatzoglou J., Williams A. (2016): Impact of anthropogenic climate change on wildfire across western US forests. Proceedings of the National Academy of Sciences of the USA, 113: 11770–11775.

Al-Dosary N.M.N., Al-Sulaiman A.M., Aboukarima M.A. (2019): Modelling the unsaturated hydraulic conductivity of a sandy loam soil using Gaussian process regression. Water SA, 45: 121–130.

Al-Dosary N.M.N., Aboukarima M.W.E.A., Marazky E.S.M. (2022): Dimensional analysis to estimate the unsaturated hydraulic conductivity of a sandy loam soil in the agricultural field. Engenharia Agrícola, 42: e20220015.

Balfour N.V., Woods W.S. (2013): The hydrological properties and the effects of hydration on vegetative ash from the Northern Rockies, USA. Catena, 111: 9–24.

Balfour N.V., Doerr H.S., Robichaud R.P. (2014): The temporal evolution of wildfire ash and implications for post-fire infiltration. International Journal of Wildland Fire, 23: 733.

Benavides-Solorio J., MacDonald L. (2001): Post-fire runoff and erosion from simulated rainfall on small plots, Colorado Front Range. Hydrological Processes, 15: 2931–2952.

Bodí B.M., Martin A.D., Balfour N.V., Santín C., Doerr H.S., Pereira P., Cerdà A., Mataix-Solera J. (2014): Wildland fire ash: Production, composition and eco-hydro-geomorphic effects. Earth-Science Reviews, 130: 103–127.

Bodi M., Doerr S., Cerda A., Mataix-Solera J. (2012): Hydrological effects of a layer of vegetation ash on underlying wettable and water repellent soil. Geoderma, 191: 14–23.

Burgy R.H., Scott V.H. (1952): Some effects of fire and ash on the infiltration capacity of soils. Transactions American Geophysical Union, 33: 405–416.

https://doi.org/10.17221/26/2026-SWR

Carsel R., Parrish R. (1988): Developing joint probability-distributions of soil-water retention characteristics. Water Resources Research, 24: 755–769.

Cerda A., Doerr S. (2008): The effect of ash and needle cover on surface runoff and erosion in the immediate post-fire period. Catena, 74: 256–263.

Cerrato J., Blake J., Hirani C., Clark A., Ali A., Artyushkova K., Peterson E., Bixby R. (2016): Wildfires and water chemistry: Effect of metals associated with wood ash. Environmental Science-Processes & Impacts, 18: 1078–1089.

Certini G. (2005): Effects of fire on properties of forest soils: A review. Oecologia, 143: 1–10.

Chaplot V., Bissonnais L.Y. (2000): Field measurements of interrill erosion under different slopes and plot sizes. Earth Surface Processes and Landforms, 25: 145–153.

Debano L.F. (2000): The role of fire and soil heating on water repellency in wildland environments: A review. Journal of Hydrology, 231–232: 195–206.

DeLong S., Youberg A., DeLong W., Murphy B. (2018): Post-wildfire landscape change and erosional processes from repeat terrestrial lidar in a steep headwater catchment, Chiricahua Mountains, Arizona, USA. Geomorphology, 300: 13–30.

Dennison P., Brewer S., Arnold J., Moritz M. (2014): Large wildfire trends in the western United States, 1984–2011. Geophysical Research Letters, 41: 2928–2933.

Doerr S. (1998): On standardizing the 'water drop penetration time' and the 'molarity of an ethanol droplet' techniques to classify soil hydrophobicity: A case study using medium textured soils. Earth Surface Processes and Landforms, 23: 663–668.

Doerr S.H., Shakesby R.A., Walsh R.P.D. (2000): Soil water repellency: Its causes, characteristics and hydrogeomorphological significance. Earth-Science Reviews, 51: 33–65.

Doerr H.S., Shakesby A.R., Dekker W.L., Ritsema J.C. (2006): Occurrence, prediction and hydrological effects of water repellency amongst major soil and land-use types in a humid temperate climate. European Journal of Soil Science, 57: 741–754.

Ebel B., Martin D. (2017): Meta-analysis of field-saturated hydraulic conductivity recovery following wildland fire: Applications for hydrologic model parameterization and resilience assessment. Hydrological Processes, 31: 3682–3696.

Ebel B., Moody J. (2017): Synthesis of soil-hydraulic properties and infiltration timescales in wildfire-affected soils. Hydrological Processes, 31: 324–340.

Ebel A.B., Moody A.J., Martin A.D. (2012): Hydrologic conditions controlling runoff generation immediately after wildfire. Water Resources Research, 48: W03529.

Fernandez C., Vega J. (2018): Evaluation of the RUSLE and disturbed WEPP erosion models for predicting soil loss in the first year after wildfire in NW Spain. Environmental Research, 165: 279–285.

Gerdes N., Webb R., Liston G., Mooney K. (2024): Evaluating the recovery of hydraulic conductivity in fire-affected soils. McNair National Research Journal, 3: 146–157.

Hallema D., Sun G., Caldwell P., Norman S., Cohen E., Liu Y., Bladon K., McNulty S. (2018): Burned forests impact water supplies. Nature Communications, 9: 1307.

Humphry J., Daniel T., Edwards D., Sharpley A. (2002): A portable rainfall simulator for plot-scale runoff studies. Applied Engineering in Agriculture, 18: 199–204.

Kim T., Lee J., Lee Y.-E., Im S. (2022): Exploring the role of ash on pore clogging and hydraulic properties of ash-covered soils under laboratory experiments. Fire, 5: 99.

Kottek M., Grieser J., Beck C., Rudolf B., Rubel F. (2006): World map of the Köppen-Geiger climate classification updated. Meteorologische Zeitschrift, 15: 259–263.

Larsen I., MacDonald L., Brown E., Rough D., Welsh M., Pietraszek J., Libohova Z., Benavides-Solorio J., Schaffrath K. (2009): Causes of post-fire runoff and erosion: Water repellency, cover, or soil sealing? Soil Science Society of America Journal, 73: 1393–1407.

Leon J., Bodi M., Cerda A., Badia D. (2013): The contrasted response of ash to wetting. The effects of ash type, thickness and rainfall events. Geoderma, 209: 143–152.

Leslie I.N., Heinse R., Smith A.M., McDaniel P.A. (2014): Root decay and fire affect soil pipe formation and morphology in forested hillslopes with restrictive horizons. Soil Science Society of America Journal, 78: 1448–1457.

Mann B.H., Whitney R.D. (1947): On a test of whether one of two random variables is stochastically larger than the other. The Annals of Mathematical Statistics, 18: 50–60.

Martinez J.R., McGuire L.A., Youberg A.M. (2025): Insights into temporal changes in debris flow susceptibility following fire in the Southwest USA from monitoring and repeat estimates of soil hydraulic and physical properties. Earth Surface Processes and Landforms, 50: e70015.

McGuire L., Rengers F., Kean J., Staley D., Mirus B. (2018): Incorporating spatially heterogeneous infiltration capacity into hydrologic models with applications for simulating post-wildfire debris flow initiation. Hydrological Processes, 32: 1173–1187.

McGuire L.A., Rengers F.K., Youberg A.M., Gorr A.N., Hoch O.J., Beers R., Porter R. (2024): Characteristics of debris-flow-prone watersheds and debris-flow-triggering rainstorms following the Tadpole Fire, New Mexico, USA. Natural Hazards Earth and System Sciences, 24: 1357–1379.

https://doi.org/10.17221/26/2026-SWR

McKenzie D., Gedalof Z., Peterson D., Mote P. (2004): Climatic change, wildfire, and conservation. Conservation Biology, 18: 890–902.

Moody J., Martin D., Haire S., Kinner D. (2008): Linking runoff response to burn severity after a wildfire. Hydrological Processes, 22: 2063–2074.

Moody J., Shakesby R., Robichaud P., Cannon S., Martin D. (2013): Current research issues related to post-wildfire runoff and erosion processes. Earth-Science Reviews, 122: 10–37.

Moody J., Ebel B., Nyman P., Martin D., Stoof C., McKinley R. (2016): Relations between soil hydraulic properties and burn severity. International Journal of Wildland Fire, 25: 279–293.

Onda Y., Dietrich W., Booker F. (2008): Evolution of overland flow after a severe forest fire, Point Reyes, California. Catena, 72: 13–20.

Pelletier J., Orem C. (2014): How do sediment yields from post-wildfire debris-laden flows depend on terrain slope, soil burn severity class, and drainage basin area? Insights from airborne-LiDAR change detection. Earth Surface Processes and Landforms, 39: 1822–1832.

Perkins P.J., Diaz C., Corbett C.S., Cerovski-Darriau C., Stock D.J., Prancevic P.J., Micheli E., Jasperse J. (2022): Multi-stage soil-hydraulic recovery and limited ravel accumulations following the 2017 Nuns and Tubbs wildfires in Northern California. Journal of Geophysical Research: Earth Surface, 127: e2022JF006591.

Rahman A., El Hayek E., Blake J., Bixby R., Ali A., Spilde M., Otieno A., Miltenberger K., Ridgeway C., Artyushkoya K., Atudorei V., Cerrato J.M.. (2018): Metal reactivity in laboratory burned wood from a watershed affected by wildfires. Environmental Science & Technology, 52: 8115–8123.

Saxe S., Hogue T., Hay L. (2018): Characterization and evaluation of controls on post-fire streamflow response across western US watersheds. Hydrology and Earth System Sciences, 22: 1221–1237.

Schmeer S., Kampf S., MacDonald L., Hewitt J., Wilson C. (2018): Empirical models of annual post-fire erosion on mulched and unmulched hillslopes. Catena, 163: 276–287.

Schoener G., Stone C.M. (2019): Impact of antecedent soil moisture on runoff from a semiarid catchment. Journal of Hydrology, 569: 627–636.

Shakesby R., Doerr S. (2006): Wildfire as a hydrological and geomorphological agent. Earth-Science Reviews, 74: 269–307.

Smith H., Sheridan G., Lane P., Nyman P., Haydon S. (2011): Wildfire effects on water quality in forest catchments: A review with implications for water supply. Journal of Hydrology, 396: 170–192.

Stoof C., Wesseling J., Ritsema C. (2010): Effects of fire and ash on soil water retention. Geoderma, 159: 276–285.

Thomaz E. (2018): Interaction between ash and soil microaggregates reduces runoff and soil loss. Science of the Total Environment, 625: 1257–1263.

Vieira D., Fernandez C., Vega J., Keizer J. (2015): Does soil burn severity affect the post-fire runoff and interrill erosion response? A review based on meta-analysis of field rainfall simulation data. Journal of Hydrology, 523: 452–464.

Watson L.C., Letey J. (1970): Indices for characterizing soil-water repellency based upon contact angle-surface tension relationships. Soil Science Society of America Journal, 34: 841–844.

Webb R.W., Litvak M.E., Brooks P.D. (2023): The role of terrain-mediated hydroclimate in vegetation recovery after wildfire. Environmental Research Letters, 18: 064036.

Westerling A.L. (2016): Corresction to "Increasing western US forest wildfire activity: Sensitivity to changes in the timing of spring". Philosophical Transactions of the Royal Society B-Biological Sciences, 371: 20160373.

Wieting C., Ebel B., Singha K. (2017): Quantifying the effects of wildfire on changes in soil properties by surface burning of soils from the Boulder Creek Critical Zone Observatory. Journal of Hydrology-Regional Studies, 13: 43–57.

Wilcoxon F. (1992): Individual comparisons by ranking methods. In: Kotz S., Johnson N.L. (eds): Breakthroughs in Statistics. Springer Series in Statistics. New York, Springer: 196–202.

Wilson C., Kampf S., Wagenbrenner J., MacDonald L. (2018): Rainfall thresholds for post-fire runoff and sediment delivery from plot to watershed scales. Forest Ecology and Management, 430: 346–356.

Woods S., Balfour V. (2008): The effect of ash on runoff and erosion after a severe forest wildfire, Montana, USA. International Journal of Wildland Fire, 17: 535–548.

Woods W.S., Balfour N.V. (2010): The effects of soil texture and ash thickness on the post-fire hydrological response from ash-covered soils. Journal of Hydrology, 393: 274–286.

Zhang R. (1997): Determination of soil sorptivity and hydraulic conductivity from the disk infiltrometer. Soil Science Society of America Journal, 61: 1024–1030.

Received: February 25, 2026
Accepted: April 16, 2025
Published online: June 1, 2026